Monthly Notices
of the
ROYAL ASTRONOMICAL SOCIETY

Mon. Not. R. Astron. Soc. **424,** 482–494 (2012) doi:10.1111/j.1365-2966.2012.21213.x

Are there any stable magnetic fields in barotropic stars?

S. K. Lander[1,2]★ and D. I. Jones[1]

[1]*School of Mathematics, University of Southampton, Southampton SO17 1BJ*
[2]*Theoretical Astrophysics, University of Tübingen, Auf der Morgenstelle 10, Tübingen 72076, Germany*

Accepted 2012 April 30. Received 2012 April 12; in original form 2012 February 21

ABSTRACT

We construct barotropic stellar equilibria, containing magnetic fields with both poloidal and toroidal field components. We extend earlier results by exploring the effect of different magnetic field and current distributions. Our results suggest that the boundary treatment plays a major role in determining whether the poloidal or toroidal field component is globally dominant. Using time evolutions we provide the first stability test for mixed poloidal–toroidal fields in barotropic stars, finding that all these fields suffer instabilities due to one of the field components: these are localized around the pole for toroidal-dominated equilibria and in the closed-field line region for poloidal-dominated equilibria. Rotation provides only partial stabilization. There appears to be very limited scope for the existence of stable magnetic fields in barotropic stars. We discuss what additional physics from real stars may allow for stable fields.

Key words: instabilities – MHD – stars: general – stars: neutron – stars: magnetic field.

1 INTRODUCTION

At least three different classes of stars appear to harbour strong and broadly similar magnetic fields: Ap/Bp stars on the main sequence, magnetic white dwarfs and neutron stars. All three classes exhibit long-lived fields, with large-scale simple structure. Surface fields are up to the order of 10^4 G for Ap/Bp stars, 10^9 G for magnetic white dwarfs and 10^{15} G for neutron stars. Although these values are very different the resultant total magnetic flux is similar for the three classes; due to their correspondingly different radii. Given their high strengths, magnetic fields are expected to play important roles in the evolution and dynamics of these stars (Wickramasinghe & Ferrario 2000; Harding & Lai 2006; Donati & Landstreet 2009). In addition, magnetic fields distort a star (Chandrasekhar & Fermi 1953); this distortion may (in a rotating neutron star) lead to appreciable emission of gravitational waves (Bonazzola & Gourgoulhon 1996).

Observations only give us direct information about the exterior field of a star, although it may be possible to infer details of the interior field of neutron stars from magnetar flares and oscillations (at present) and through gravitational-wave emission (in the future). Having no direct probe of the interior is a problem, since the details of the field geometry can greatly affect the ratio of internal-to-external field strength; the observed field may provide a poor estimate of the global value. For example, if a star's magnetic field is confined to an outer region (like the crust of a neutron star), its volume-averaged value could be lower than expected from the observed surface value; if the field is predominantly buried within the star, its strength may be greater than expected. Innumerable studies have been motivated by the attempt to understand the kinds of magnetic field that may exist in stars (see Mestel 1999, for a review).

One approach to the modelling of stellar magnetic fields is to construct equilibrium configurations of a fluid star and then to show that they are dynamically stable (and hence credible models for the long-lived magnetic fields present in many real stars). In practice, the latter step is very difficult – it requires confirmation that *every* possible perturbation about a stellar equilibrium is stable. For the former step, constructing hydromagnetic equilibria, virtually all studies make the simplifying assumption of a barotropic (i.e. unstratified) stellar model: the pressure is taken as a function of density alone. This has been criticized as unrealistic – temperature/entropy profiles provide stratification in main-sequence stars (Mestel 1956) and white dwarfs (Reisenegger 2009), whilst the varying proportions of charged particles (composition gradients) result in neutron star stratification (Reisenegger & Goldreich 1992). Stratification provides an additional degree of stabilization, and numerical simulations for main-sequence stars with entropy gradients have provided strong evidence for the existence of stable magnetic equilibria in this case (Braithwaite & Nordlund 2006; Braithwaite 2009). It is not clear if this result is applicable to neutron stars, however, where the origin of the stratification is different.

Despite its limitations, a barotropic equation of state is a sensible first approximation to stellar matter, and one which is astrophysically relevant if it allows for stable magnetic equilibria. It is still unknown whether such stable configurations exist, but there seem to be two reasons to expect them to. The first is connected with the

★E-mail: samuel.lander@uni-tuebingen.de

© 2012 The Authors
Monthly Notices of the Royal Astronomical Society © 2012 RAS

Downloaded from http://mnras.oxfordjournals.org/ at University of Southampton on January 5, 2017

geometry of a mixed poloidal–toroidal field. A poloidal field is known to be unstable in the region where its field lines close within the star, whilst a toroidal field suffers localized instabilities around the pole; in a mixed field, each field component 'fills in' the region where the other field component is unstable. This changes the magnetic field geometry in these unstable regions, potentially suppressing the instabilities (Wright 1973; Tayler 1980). The second reason to expect stable equilibria is that the 'twisted-torus' fields found for barotropic equilibria (Ciolfi et al. 2009; Lander & Jones 2009) are qualitatively similar to the final state of the nonlinear stratified-star simulations mentioned above (Braithwaite & Nordlund 2006).

This paper aims to explore the possibility of stable magnetic fields existing in barotropic stars by testing the stability of a number of equilibrium models. We begin, in Section 2, by exploring the range of magnetic equilibria possible in barotropic stars, reviewing the key equations of the problem and examining the various classes of solution. Broadly, the resulting equilibria differ in how their magnetic field and current are distributed. In Section 3, we discuss properties of perturbations in a magnetic star: the governing equations, how a mixed poloidal–toroidal field breaks the equatorial symmetry of the perturbations and potential instabilities. Next, we use the mixed-field equilibria of Section 2 as background configurations for time evolutions of the linearized perturbation equations (Section 4). We study perturbations known to result in instabilities for purely poloidal/toroidal fields to determine whether or not these perturbations are still unstable in mixed-field stars. Following this, we discuss some important aspects of stellar physics not accounted for in barotropic models, and whether these may remove magnetic instabilities (Section 5). Finally, in Section 6 we summarize our results.

2 MIXED-FIELD BAROTROPIC EQUILIBRIA

The first step towards studying the stability of magnetized stars is to construct suitable background equilibrium models, which we describe in this section. Although full details may be found in Lander & Jones (2009), we pause here to focus on the key equations of the problem and any restrictions imposed by our assumptions. This is important, since our aim is to produce the widest possible range of equilibrium models to test for stability.

We model a star as a perfectly conducting barotropic fluid body, in Newtonian gravity and axisymmetry. The star has a mixed poloidal–toroidal magnetic field $\boldsymbol{B}$, and our scheme also allows for rigid rotation (about the magnetic symmetry axis) with angular velocity Ω. We work in cylindrical polar coordinates (ϖ, ϕ, z), with the z-axis being aligned with the symmetry axis of the star. An equilibrium is described by the stationary form of the magnetohydrodynamics (MHD) Euler equation:

$$\frac{\nabla P}{\rho} + \nabla\Phi - \nabla\left(\frac{\varpi^2\Omega^2}{2}\right) - \frac{\boldsymbol{j}\times\boldsymbol{B}}{\rho} = 0, \tag{1}$$

where P is fluid pressure, ρ mass density, Φ gravitational potential and $\boldsymbol{j}$ the electric current. This equation needs to be solved together with Ampère's law,

$$4\pi\boldsymbol{j} = \nabla\times\boldsymbol{B}, \tag{2}$$

Poisson's equation,

$$\nabla^2\Phi = 4\pi G\rho, \tag{3}$$

where G is the gravitational constant, and the solenoidal constraint on the magnetic field,

$$\nabla\cdot\boldsymbol{B} = 0. \tag{4}$$

The system is closed with an equation of state. We choose a polytrope with index $N = 1$, a typical approximation for neutron star matter:

$$P = P(\rho) = k\rho^{1+1/N} = k\rho^2. \tag{5}$$

Note that a more suitable value for white dwarfs would be $N = 1.5$, whilst main-sequence stars tend to be modelled as $N = 3$ polytropes. We are able to generate magnetic equilibria for a variety of values of N (Lander & Jones 2009), but the resulting field configurations are all qualitatively similar. Since magnetic field instabilities are related to the geometry of the field (see Section 3.3), we have some expectation that our results for $N = 1$ should be representative of the stability of barotropic main-sequence stars and white dwarfs, not just neutron stars.

Some algebra is needed to recast the equilibrium equations above into a convenient form for solution. First let us take the curl of the Euler equation (1), which – in the case of a *barotropic* star – yields

$$\frac{\boldsymbol{j}\times\boldsymbol{B}}{\rho} = \nabla M, \tag{6}$$

for some scalar function M. The solenoidal constraint on the magnetic field together with the assumption of axisymmetry allows us to express the poloidal field component $\boldsymbol{B}_{\rm pol}$ in terms of a stream function u:

$$\boldsymbol{B}_{\rm pol} = \frac{1}{\varpi}\nabla u\times\boldsymbol{e}_\phi. \tag{7}$$

Furthermore, the toroidal component is related to the stream function through some function f,

$$B_\phi = \frac{1}{\varpi}f(u), \tag{8}$$

and it may also be shown that $M = M(u)$. Therefore, the magnetic field and the force it exerts on the fluid are both related to the single scalar function u. Equivalently, it is possible to work with the ϕ-component of the magnetic vector potential $\boldsymbol{A}$ instead, since $u = \varpi A_\phi$. With various algebraic tricks, one may derive a relation between these functions u, M and f, known as the Grad–Shafranov equation (Grad & Rubin 1958; Shafranov 1958):

$$-4\pi\rho\varpi^2\frac{\mathrm{d}M}{\mathrm{d}u} = f\frac{\mathrm{d}f}{\mathrm{d}u} + \left(\frac{\partial^2}{\partial\varpi^2} - \frac{1}{\varpi}\frac{\partial}{\partial\varpi} + \frac{\partial^2}{\partial z^2}\right)u. \tag{9}$$

Combining the Grad–Shafranov equation with Ampère's law (2) in axisymmetry yields a useful relation between the magnetic functions, the current and the field:

$$\boldsymbol{j} = \frac{1}{4\pi}\frac{\mathrm{d}f}{\mathrm{d}u}\boldsymbol{B} + \rho\varpi\frac{\mathrm{d}M}{\mathrm{d}u}\boldsymbol{e}_\phi. \tag{10}$$

By rewriting $\boldsymbol{j}$ and $\boldsymbol{B}$ in terms of the stream function (Tomimura & Eriguchi 2005), we arrive at a version of Poisson's equation for the magnetic field:

$$\nabla^2\left(\frac{1}{\varpi}u\sin\phi\right) = -\left(\frac{f}{\varpi}\frac{\mathrm{d}f}{\mathrm{d}u} + 4\pi\varpi\rho\frac{\mathrm{d}M}{\mathrm{d}u}\right)\sin\phi. \tag{11}$$

The above result is the last that one can obtain without loss of generality. For numerical solution, we now need an integral form of equation (11), and in choosing a Green's function to produce this integral we also implicitly choose a boundary condition for

Downloaded from http://mnras.oxfordjournals.org/ at University of Southampton on January 5, 2017

the exterior field. All of the equilibria we generate use the integral equation

$$\frac{1}{\varpi}u\sin\phi = \frac{1}{4\pi}\int \frac{f'(\tilde{u})f(\tilde{u})/\tilde{\varpi} + 4\pi\tilde{\varpi}\,\tilde{\rho}M'(\tilde{u})}{|\boldsymbol{r}-\tilde{\boldsymbol{r}}|}\sin\tilde{\phi}\,\mathrm{d}\tilde{\boldsymbol{r}}, \quad (12)$$

for which the magnetic field magnitude falls off as a dipole, $B \to 1/r^3$ as $r \to \infty$. If one wished instead to solve for fields confined within the star (for example), a modified Green's function would be necessary.

One must also specify the functional forms of $M(u)$ and $f(u)$, which are chosen on physical grounds. In particular, we see from equation (10) that the derivatives $M'(u)$ and $f'(u)$ are related to the distribution of electric current. Both M and f can be chosen to allow for smooth or discontinuous current distributions inside the star, whilst most choices for f result in currents outside the star. As discussed later, the limited choices of $f(u)$ which avoid exterior currents all produce qualitatively similar equilibria.

The integral equations for Φ and u are solved together with the Euler equation using a numerical scheme which iteratively finds equilibrium configurations – for details see Lander & Jones (2009) or Tomimura & Eriguchi (2005). For numerical solution, it is convenient to use dimensionless variables, which we denote by a hat (e.g. $\hat{\Omega}$). We produce these by dividing each physical quantity by the requisite combination of powers of G, maximum density $\rho_{\max}$ and equatorial radius $r_{\rm eq}$. The results of this section are presented in dimensionless form to avoid specializing to a specific star. In addition, the important features of the equilibria – the distribution and relative strength of the two field components – are clear without redimensionalizing. We now consider different choices of the two magnetic functions $f(u)$ and $M(u)$ and the resultant equilibria.

2.1 Exterior poloidal field, no surface currents: 'type 1'

Our first choice of surface treatment is that employed in Lander & Jones (2009). Specifically, the toroidal component is confined within the star and goes to zero smoothly at its surface, whilst the internal poloidal field matches smoothly to an external component, which falls off as $1/r^3$. We feel this is the most natural boundary condition for a fluid star in vacuum, although it ignores the different physics present in the outer regions of stars – for example, the crust, ocean and magnetosphere of a neutron star. One surprising, perhaps unsatisfactory, aspect of these solutions is that we find the toroidal component is always weak with respect to the poloidal one in a global sense; its contribution $\mathcal{E}_{\rm tor}$ to the magnetic energy $\mathcal{E}_{\rm mag}$ is never more than a few per cent of the total. Locally the two field components can be more similar, however, with the maximum values of poloidal and toroidal components being of comparable magnitude.

To produce the desired surface behaviour of the toroidal field component, we need to make a suitable choice of magnetic function $f(u)$. We take

$$f(u) = \begin{cases} a(u-u_{\rm surfmax})^{1.1} & u > u_{\rm surfmax}, \\ 0 & u \le u_{\rm surfmax}, \end{cases} \quad (13)$$

where $u_{\rm surfmax}$ is the maximum surface value attained by u, as discussed by various authors (Tomimura & Eriguchi 2005; Lander & Jones 2009; Ciolfi, Ferrari & Gualtieri 2010; Lyutikov 2010) and a is a constant coefficient related to the relative strength of toroidal and poloidal components ($a = 0$ produces a purely poloidal field). Experimenting with different exponents of $(u - u_{\rm surfmax})$, we have found that lower values allow for slightly stronger toroidal components. At the same time, we wish to avoid producing a step in $f'(u)$, so we need the exponent to be greater than unity; hence we chose it as 1.1. In other cases the equilibria are still qualitatively similar. The functional form (13) has the effect of enclosing the toroidal field component within the closed-field line region of the star, producing equilibria where the toroidal field only occupies a small volume of the star. Nonetheless, it is the largest volume that does not give rise to an exterior current.

Within an iterative scheme, we consider this choice slightly inconsistent with the requirement that f be a function of u alone: $u_{\rm surfmax}$ is a constant, but one found by evaluating u at $\rho = 0$. The value of $u_{\rm surfmax}$ varies between iterative steps, and hence the scheme involves an implicit density dependence. Instead, it is possible to produce entirely consistent equilibria using the stream function's global maximum $u_{\rm globmax}$ (which is attained within the star): one can fit the f function to contours of different fractions of $u_{\rm globmax}$ and pick the solution with the largest volume of toroidal component which does not extend outside the star. The resulting equilibria appear identical to those using $u_{\rm surfmax}$, however, suggesting that (13) is in fact an acceptable choice.

All of our type 1 equilibria use the above choice for f, but differ in the choice of the other magnetic function M. In Lander & Jones (2009) we found that only $M(u) = \kappa u$ (where κ is a constant) produced magnetized equilibria, with other cases resulting in our numerical scheme iterating to unmagnetized solutions; here we refer to the $M = \kappa u$ equilibria as type 1a. Physically, κ gives the relative strength of the Lorentz force compared with gravity and is thus related to the magnetic field strength; setting $\kappa = 0$ produces an unmagnetized star.

More recently, we have found a way of using other functional forms of M without the numerical scheme iterating to a zero-field solution. By including a $1/u_{\rm globmax}$ factor, the field at each iterative step is 'normalized' to the same magnitude as the previous step and not driven to zero. These different functional forms of M produce qualitatively similar equilibria, so we take one representative example – $M = \kappa u^2/u_{\rm globmax}$ – and refer to it as type 1b.

A different generalization of the original type 1a equilibria is to relax the requirement that the current density be continuous inside the star. Allowing for steps in the current means we can choose forms of M and f with discontinuous u-derivatives. We find that a step in $f'(u)$ produces little qualitative difference in equilibria from types 1a or 1b, so we do not consider these further. More significant differences emerge by choosing a step in $M'(u)$ – as an example of these we choose the following:

$$M'(u) = \begin{cases} \kappa & u > u_{\rm surfmax}, \\ 0 & u \le u_{\rm surfmax}. \end{cases} \quad (14)$$

Note that this corresponds to a step in the interior current, but not to a surface current; see equation (10). Since we wish to avoid δ-distribution behaviour of $M'(u)$ (and hence the Lorentz force) in this class of solutions, however, we must ensure that M itself is smooth – and so we take

$$M(u) = \begin{cases} \kappa(u-u_{\rm surfmax}) & u > u_{\rm surfmax}, \\ 0 & u \le u_{\rm surfmax}. \end{cases} \quad (15)$$

This choice confines the Lorentz force within the closed-field line region, with a force-free field existing in the rest of the stellar interior as well as the exterior. The other magnetic function f is chosen in the same way as for type 1a. This final choice we refer to as type 1c.

The three type 1 field configurations are compared in Fig. 1, where we plot the variation in magnitude of B_r, B_θ and B_ϕ with

Downloaded from http://mnras.oxfordjournals.org/ at University of Southampton on January 5, 2017

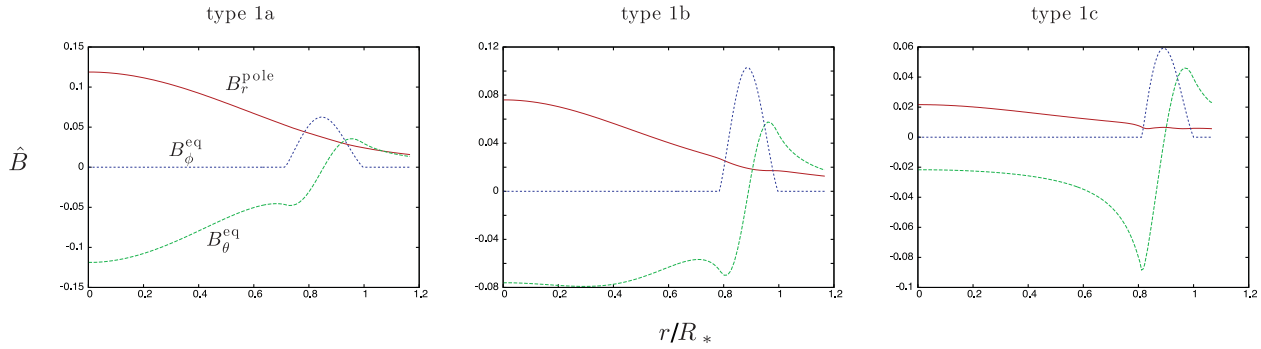

Figure 1. Three different type 1 or 'twisted-torus' equilibria, all with a relatively large toroidal component: $\mathcal{E}_{\rm tor}/\mathcal{E}_{\rm mag} = 3$, 4.5 and 4.5 per cent for types 1a, 1b and 1c, respectively. The variation in magnitude of the three field components is shown as a function of dimensionless stellar radius r/R_*, where R_* is the surface of the star. B_θ and B_ϕ are evaluated along the equatorial axis, whilst B_r (zero along this axis) is evaluated along the polar axis. The neutral line of the poloidal component is located where the B_θ line crosses the x-axis, and the toroidal component is centred around this line. These three equilibria represent the range of solutions we have found which have an exterior field but no surface/exterior current; nonetheless, all are qualitatively similar.

stellar radius. The maximum value attained by the toroidal field is greater in type 1b than in type 1a, but it is still confined to the same small region. The profiles of types 1a and 1c differ mainly in the relatively weak radial field in type 1c. Overall, however, the three field configurations appear very similar.

2.2 Confined fields, no exterior poloidal component: 'type 2'

Next, we consider a very different class of equilibrium from that of the previous subsection: one where the magnetic field is confined to the stellar interior. We will refer to such confined-field equilibria as 'type 2'. As described earlier, the boundary condition on the magnetic field is imposed by the choice of Green's function used to solve equation (11); to generate equilibria with confined fields we would need to modify this function. Since the total magnetic field vanishes at the stellar surface in this case, there would be no separate need to ensure that the toroidal field vanishes outside the star.

The major disadvantage in assuming a confined field is the more limited astrophysical relevance: in particular, many stars have strong exterior magnetic fields, thought to be comparable in strength with the internal value. One possible application of this treatment could be to model accreting neutron stars or white dwarfs, where the surface field is weak but a strong internal field could still exist, 'buried' under the accreted matter.

There are interesting differences between the properties of magnetic equilibria in the confined and non-confined cases. The non-confined models described above (type 1) are 'poloidal-dominated' – the poloidal field component contains most of the star's magnetic energy – whilst confined-field solutions seem to be toroidal-dominated by the same measure (Ioka 2001; Haskell et al. 2008; Duez & Mathis 2010). Related to this, type 1 magnetic fields induce oblate distortions in the star's density distribution, whereas type 2 equilibria have prolate ellipticities. Finally, since the magnetic fields in the two cases are qualitatively different, it is natural to expect them to have different stability properties.

Generating confined-field equilibria would not be a straightforward extension to our work, nor is there strong motivation to do so from observations. On the other hand, we would like to compare the two contrasting field geometries of type 1 and type 2 equilibria. To this end, we turn to the perturbative semi-analytic models in section B2 of Haskell et al. (2008) for confined mixed-field stars. Their magnetic field (in spherical polar coordinates) is of the form

$$\boldsymbol{B} = \frac{2A\cos\theta}{r^2}\boldsymbol{e}_r - \frac{A\sin\theta}{r}\boldsymbol{e}_\theta + \frac{\pi\lambda A\sin\theta}{rR_*}\boldsymbol{e}_\phi, \tag{16}$$

with A a radial function given by

$$A(r) = \frac{B_k R_*^2}{(\lambda^2-1)^2 y}\left[2\pi\frac{\lambda y\cos(\lambda y)-\sin(\lambda y)}{\pi\lambda\cos(\pi\lambda)-\sin(\pi\lambda)} + [(1-\lambda^2)y^2-2]\sin y + 2y\cos y\right], \tag{17}$$

where $y = \pi r/R_*$ and B_k is a constant governing the field strength. By demanding that the exterior field vanish and the interior field be finite and continuous, this becomes an eigenvalue problem to solve for λ, with only a discrete set of solutions being admissible. Higher eigenvalues correspond to a stronger toroidal component with an increasing number of nodes. Haskell et al. (2008) found that the lowest eigenvalue solution for the magnetic field was $\lambda = 2.362$, corresponding to a nodeless toroidal component. We adopt this field configuration together with a spherical density distribution as our 'type 2' equilibrium, neglecting the (small) distorting effect of the magnetic field. Unlike our type 1 equilibria, this is not fully self-consistent, but the resulting models should be accurate enough for a qualitative idea of stability.

We plot this 'type 2' magnetic field in Fig. 2. Even for this lowest eigenvalue solution, the toroidal component magnetic energy

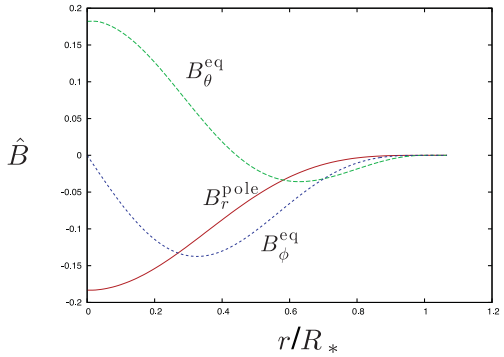

Figure 2. A type 2 equilibrium, where all field components are confined within the star, not just B_ϕ. Plotted here is the lowest eigenvalue solution of Haskell et al. (2008), corresponding to no nodes in the toroidal field. 65 per cent of the magnetic energy is contained in the toroidal component – far higher than for type 1 equilibria.

Downloaded from http://mnras.oxfordjournals.org/ at University of Southampton on January 5, 2017

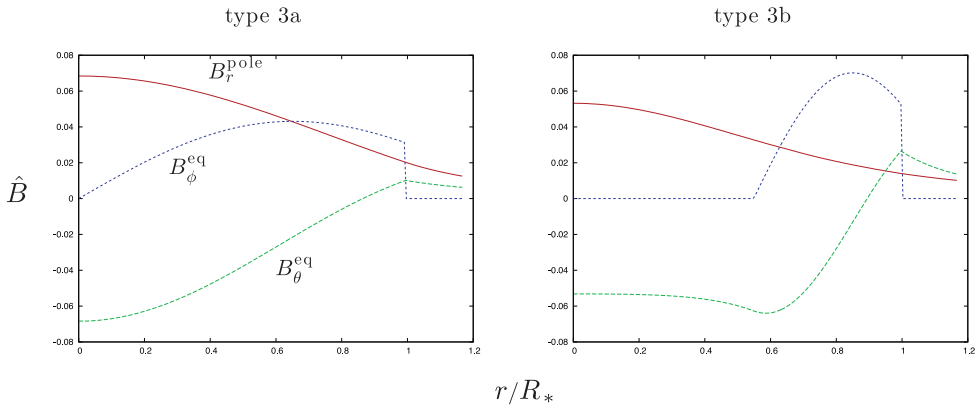

Figure 3. Equilibria with the toroidal field component matched to a surface current rather than going smoothly to zero there. For the type 3a model, $\mathcal{E}_{\rm tor}/\mathcal{E}_{\rm mag} = 50$ per cent; for type 3b it is 30 per cent. The right-hand plot is an attempt to produce an equilibrium with a surface current that also looks roughly like a twisted-torus structure.

is 65 per cent of the total.[1] Clearly, the toroidal field is far more significant globally than for type 1 equilibria, extending throughout the stellar interior.

2.3 Exterior poloidal component, surface currents: 'type 3'

The types of magnetic field outlined in the last subsections represent two extremes of mixed-field equilibria with a confined toroidal component; in type 1 the poloidal component is non-zero across the surface and into the exterior, whilst in type 2 it vanishes at the surface. For both types, the toroidal component goes to zero smoothly at the surface. Type 1 equilibria are always dominated by the poloidal component and type 2 equilibria by the toroidal component. Since we wish to test the dependence of stability on the relative strength of the two field components, we would like a way of introducing a 'sliding scale' between types 1 and 2 to produce equilibria with more equal proportions of each field component.

As a way to produce mixed-field equilibria with stronger toroidal components as well as an exterior field, we consider equilibria with surface currents in this subsection. We stress that we are not asserting that surface currents themselves are necessarily significant in real stars – they simply provide a mathematically convenient way of producing a surface boundary condition which is different from that of the type 1 or type 2 equilibria discussed above. There is some motivation for employing a boundary condition 'in between' that of types 1 and 2, however: in the outer region of a star, the mass density becomes very low and the resistivity increases, so deviations may be expected from an ideal-MHD treatment. Furthermore, modelling a neutron star as a fluid body in vacuum neglects the effect of its crust, ocean and magnetosphere. A first, crude attempt to account for these differences could be to modify the boundary condition at the stellar surface, which may mathematically (though not physically) resemble a surface current.

For these equilibria we choose a form of f such that B_ϕ is non-zero up to the stellar surface. An exterior toroidal field requires an exterior current; since we still want to avoid this, we appeal to some (poloidal) surface current to match the non-zero interior toroidal field to a zero exterior one. This surface current is not separately modelled; its form is whatever required to produce a consistent matching for the toroidal field component. A similar approach to the construction of magnetic equilibria was taken by Colaiuda et al. (2008). We caution the reader that this surface current will, in general, induce an azimuthal component of the Lorentz force at the surface; in reality, this would need to be balanced by other physics beyond our fluid star model. In practice, for this class of equilibria only the form of the magnetic function f is changed. One simple choice is

$$f'(u) = \begin{cases} a & \text{interior,} \\ 0 & \text{exterior,} \end{cases} \tag{18}$$

$$f(u) = \begin{cases} au & \text{interior,} \\ 0 & \text{exterior,} \end{cases} \tag{19}$$

which we refer to as type 3a. Note that since $f(u) = \varpi B_\phi$, this corresponds to a jump in the toroidal field component at the stellar surface.

The toroidal field is now distributed throughout the stellar interior. As a half-way choice between this type of equilibrium and the usual twisted-torus structures of type 1 (where the toroidal field only exists in some small torus near the surface), we consider one final class of equilibrium – type 3b – designed to look like a twisted-torus configuration but with a larger torus than in type 1. Again, we use a surface current to achieve this:

$$f'(u) = \begin{cases} a & \text{interior and } u > 0.5u_{\rm surfmax}, \\ 0 & \text{otherwise,} \end{cases} \tag{20}$$

$$f(u) = \begin{cases} a(u - 0.5u_{\rm surfmax}) & \text{interior and } u > 0.5u_{\rm surfmax}, \\ 0 & \text{otherwise.} \end{cases} \tag{21}$$

The relative magnitudes of the r, θ and ϕ components of the magnetic field in these surface-current equilibria are plotted in Fig. 3. Type 3a equilibria look quite similar to the confined-field solution in Fig. 2, differing mostly near the surface, since the surface-current equilibria have exterior fields. The type 3b equilibrium was constructed to resemble a twisted-torus (i.e. type 1) equilibrium, but with a larger toroidal component (cf. Fig. 1).

We conclude this section by comparing the various magnetic equilibrium models we have constructed. In Fig. 4 we plot poloidal-field lines and represent the toroidal component magnitude with coloured shading. Since the three type 1 equilibria are rather similar, we include only one of these (type 1a) as a representative example.

[1] Table 1 from Haskell et al. (2008) indicates that $\mathcal{E}_{\rm tor}/\mathcal{E}_{\rm mag} = 90$ per cent, due to a normalization error: their averaged poloidal field is $\sim 2.2 \times 10^{12}$ G, not 1×10^{12} G as reported.

Downloaded from http://mnras.oxfordjournals.org/ at University of Southampton on January 5, 2017

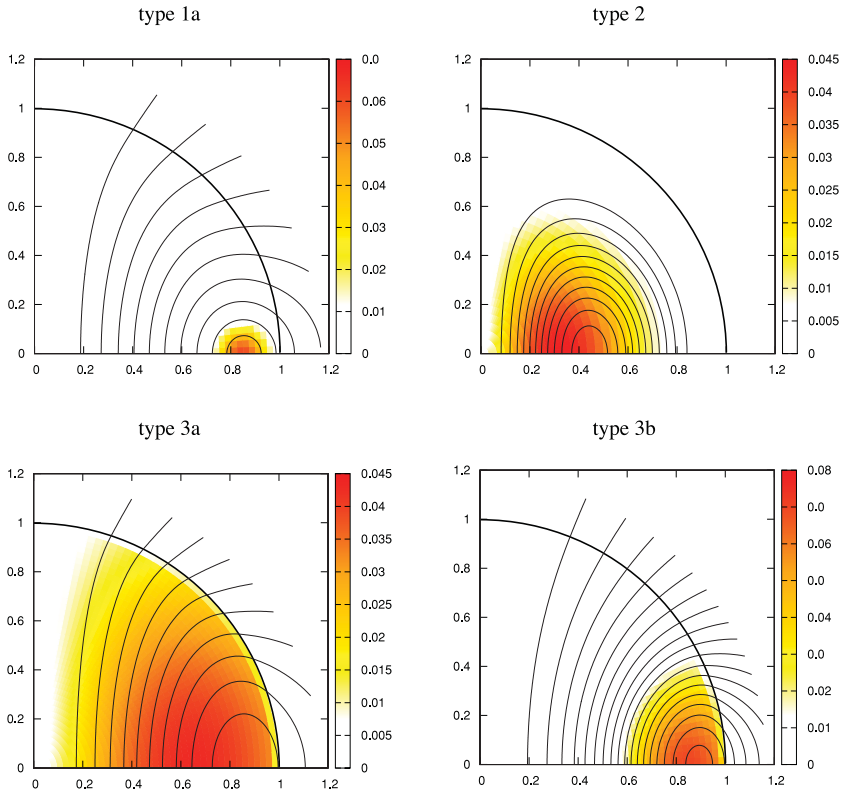

Figure 4. Comparison of various magnetic field equilibrium structures. The poloidal field lines are shown in black, whilst the strength of the toroidal field is represented by the colour code. The black arc from $x = 1$ to $y = 1$ is the stellar surface. Type 1a is a typical 'twisted-torus' configuration, where the toroidal field component sits inside the closed field lines. The other field configurations do not have this twisted-torus geometry. Type 2 is a confined field, so all poloidal field lines close within the star, whilst types 3a and 3b are equilibria with surface currents.

3 PERTURBATIONS OF A MIXED-FIELD STAR

3.1 Perturbation equations and numerics

Given the apparently intractable nature of the analytic problem (Tayler 1980), we will study the stability of mixed poloidal–toroidal field stars using a numerical approach. Our code evolves the linearized MHD perturbation equations, taking the equilibria of the previous section as background configurations. We have successfully used this code to study instabilities in stars with purely toroidal fields (Lander & Jones 2011a) and purely poloidal fields (Lander & Jones 2011b), and so expect its results for mixed fields to be reliable. Since full details of our numerical scheme are reported in Lander, Jones & Passamonti (2010), we content ourselves with a brief summary of the salient details here.

We wish to study the behaviour of linear perturbations about MHD equilibrium; this allows us to test the stability of the equilibrium, based on whether or not we find unstable modes of the system. We work in the Cowling approximation, where perturbations in the gravitational potential are not evolved. This approximation is known to overestimate the stability of a system (Moss & Tayler 1969), placing some potential doubt over any magnetic fields we find to be stable, but *not* over those systems we find to be unstable.

Instead of working directly with the velocity $\boldsymbol{v}$ and the perturbed magnetic field $\delta\boldsymbol{B}$, we define flux variables $\boldsymbol{f} \equiv \rho_0\boldsymbol{v}$ and $\beta \equiv \rho_0\delta\boldsymbol{B}$ (zero subscripts denote background quantities). This allows for a simpler, more numerically stable treatment of the stellar surface. Our final perturbation variable is the perturbed density $\delta\rho$. Now, in the frame corotating with the background star, the linear perturbations of the system are described by the following time-evolution equations:[2]

$$\frac{\partial \boldsymbol{f}}{\partial t} = -\frac{\gamma P_0}{\rho_0}\nabla\delta\rho + \frac{(2-\gamma)\nabla P_0}{\rho_0}\delta\rho - 2\boldsymbol{\Omega}\times\boldsymbol{f} - \frac{\delta\rho}{4\pi\rho_0}(\nabla\times\boldsymbol{B}_0)\times\boldsymbol{B}_0 + \frac{1}{4\pi\rho_0}(\nabla\times\boldsymbol{B}_0)\times\beta + \frac{1}{4\pi\rho_0}(\nabla\times\beta)\times\boldsymbol{B}_0 - \frac{1}{4\pi\rho_0^2}(\nabla\rho_0\times\beta)\times\boldsymbol{B}_0, \quad (22)$$

$$\frac{\partial\delta\rho}{\partial t} = -\nabla\cdot\boldsymbol{f}, \quad (23)$$

$$\frac{\partial\beta}{\partial t} = \nabla\times(\boldsymbol{f}\times\boldsymbol{B}_0) - \frac{\nabla\rho_0}{\rho_0}\times(\boldsymbol{f}\times\boldsymbol{B}_0). \quad (24)$$

This 3D system of equations may be reduced to 2D, using the axisymmetry of the background to decompose in the azimuthal angle ϕ. The desired azimuthal index m is chosen at the outset of each evolution, which is convenient for studying the stability of particular modes. Imposing the perturbations' symmetries at the poles then reduces our numerical grid to one half-disc. For a purely poloidal or purely toroidal field, equatorial symmetries allow a further reduction of the grid to a single quadrant of a disc, but these symmetries

[2] Note that in our earlier papers using this time evolution code, an algebra error affected the Coriolis term of the perturbed Euler equation as printed. The equations used in the code were, however, correct.

Downloaded from http://mnras.oxfordjournals.org/ at University of Southampton on January 5, 2017

are broken in the presence of a mixed poloidal–toroidal field, for which a half-disc grid is required; see the next subsection.

Each evolution is started with either an f- or r-mode eigenfunction as initial data; each excites a different symmetry class of perturbations (next subsection). The code then evolves the perturbation equations using a predictor–corrector algorithm, and is second-order convergent. We include artificial viscosity – a fourth-order Kreiss–Oliger dissipation term added to the Euler equation – but take care to do so at the minimum value required to damp numerical instabilities, so physical instabilities are minimally affected. No corresponding artificial resistivity term was added to the induction equation. To prevent growth of $\nabla \cdot \boldsymbol{B}$ errors, we employ an auxiliary variable and equation for divergence cleaning (Dedner et al. 2002). As for the background models, we non-dimensionalize variables here using a combination of G, $\rho_{\max}$ and $r_{\rm eq}$. Generally we present results in dimensionless variables, since the important features of our evolutions are qualitative – the presence or absence of dynamical instabilities – rather than quantitative.

3.2 The importance of equatorial symmetry

The equatorial symmetry of perturbations is closely related to the behaviour of modes and instabilities in magnetic stars. Here we explore this important aspect of the perturbation problem and introduce some useful notation for later.

Let us start with the behaviour of perturbations of an unmagnetized fluid star. For this case, the four perturbation variables split into two sets based on their shared symmetry properties; we denote these sets $S_1 \equiv \{f_r, f_\phi, \delta\rho\}$ and $S_2 \equiv \{f_\theta\}$. For example, an initial perturbation in f_r which is symmetric (or 'even') about the equator will induce corresponding symmetric perturbations in f_ϕ and $\delta\rho$, but an *antisymmetric* f_θ perturbation. A different initial perturbation, leading to equatorially antisymmetric behaviour of the perturbations in class S_1, would produce symmetric perturbations in the S_2 element.

From this, we can define two symmetry classes for modes (coherent global responses of the fluid). The first we refer to as $\mathcal{P}^+$, and corresponds to S_1 elements being even and S_2 elements odd; the other class, $\mathcal{P}^-$, is that of odd S_1 elements and even S_2 elements. Note that the $\mathcal{P}^+$ class is equivalent to the set of modes variously called polar, polar-led or spheroidal – for example, the f mode. The $\mathcal{P}^-$ class is the set of modes known as axial/axial-led/toroidal, the most familiar example being the r mode.

If we now add a purely poloidal magnetic field to the background, an analysis of the equations shows that the original S_1 and S_2 classes are augmented by magnetic variables in the following manner: $S_1 \equiv \{f_r, f_\phi, \delta\rho, \beta_\theta\}$ and $S_2 \equiv \{f_\theta, \beta_r, \beta_\phi\}$. The chief instability for a purely poloidal field is a kink mode in the closed-field line region, as described in the next subsection. This corresponds to motion in the θ-direction across the equator and hence to a *symmetric* perturbation there; an antisymmetric v_θ is zero along the equator. For this reason the instability occurs only in the $\mathcal{P}^-$ symmetry class, and its development can be prevented in evolutions which enforce $\mathcal{P}^+$ conditions at the equator.

In the case of a star with a purely *toroidal* magnetic field, the division of perturbations based on equatorial symmetry changes from the poloidal-field case, and the two sets become $S_1 \equiv \{f_r, f_\phi, \delta\rho, \beta_r, \beta_\phi\}$ and $S_2 \equiv \{f_\theta, \beta_\theta\}$. Since S_1 and S_2 take different forms in the purely poloidal and purely toroidal cases, it follows that when the background has a mixed poloidal–toroidal field, the equatorial symmetry of the perturbations will be lost. As a result, we will no longer have a division into $\mathcal{P}^+$ and $\mathcal{P}^-$ classes, and instead the two will be 'coupled' through the magnetic field. Equally, there will no longer be distinct axial-led or polar-led modes in the conventional use of the terms.

3.3 Diagnosing instability

Both purely poloidal and purely toroidal magnetic fields are susceptible to rapidly developing instabilities, of essentially the same origin: the unstable nature of a cylindrical plasma column. Temporarily neglecting gravity, the simplest instabilities of the cylindrical system are the sausage or varicose mode and the kink mode, illustrated in Fig. 5 (left-hand side). Based on this, one can identify regions of a star where magnetic instabilities may occur: the cylindrical region around the pole for a toroidal field and the torus around a poloidal field's neutral line (i.e. the line along which the poloidal field vanishes). Any such instabilities will be related to the geometry of the magnetic field, so should be present even for weak fields, albeit with slower growth rates (Markey & Tayler 1973; Tayler 1973; Wright 1973).

We now turn to the right-hand side of Fig. 5, and consider first a star with a purely toroidal magnetic field. The geometry is similar to that of the cylindrical plasma, but the star's self-gravity must now be accounted for. Since both sausage and kink instabilities in this case can operate parallel to shells of constant gravitational potential, however, neither should be suppressed; accordingly, we expect $m = 0$ and 1 magnetic instabilities to exist.[3] In a poloidal field the geometry is different, with the unstable cylinder closed into a torus, resulting in potential instability in all $m > 0$ perturbations. The sausage mode of the cylinder, on the other hand, is suppressed by gravity; so we do not expect a significant $m = 0$ instability for a poloidal-field star.

For a mixed poloidal–toroidal field to be stable, we need to check that all instabilities that occur for a purely poloidal or toroidal field are eliminated in the mixed configuration (and that no new instabilities arise). In this paper, we only consider non-axisymmetric modes. To test for any instabilities due to the toroidal component, therefore, we look at the behaviour of $m = 1$ perturbations in the vicinity of the pole. By contrast, we anticipate that instabilities of the poloidal component will be localized in the closed-field line region, for any $m \geq 1$. For a purely poloidal field only $\mathcal{P}^-$ initial data will produce these (kink) instabilities, but a mixed field allows for $\mathcal{P}^+$–$\mathcal{P}^-$ coupling – so that any initial data may result in the excitation of a poloidal-component instability.

In the initial phase of an instability, an unstable mode is excited with an amplitude which grows exponentially in time; to study this, it is sufficient to consider the behaviour of linear perturbations about an equilibrium. Beyond some amplitude the mode 'saturates', causing a non-linear rearrangement of the magnetic field for which the perturbative regime is no longer applicable. Since we only evolve the linearized system, however, the background is stationary and experiences no reduction in magnetic energy as the amplitude of a perturbation grows – hence the instability is able to grow indefinitely. This is clearly not realistic, but it does allow us to determine the growth rate of the initial instability with ease. In all cases, the onset time of the instability is expected to correspond to the time

[3] In the special case of an incompressible star, the sausage mode *does* have to move fluid elements along the z-axis and hence will be suppressed by gravity, but the $m = 1$ instability will remain.

Downloaded from http://mnras.oxfordjournals.org/ at University of Southampton on January 5, 2017

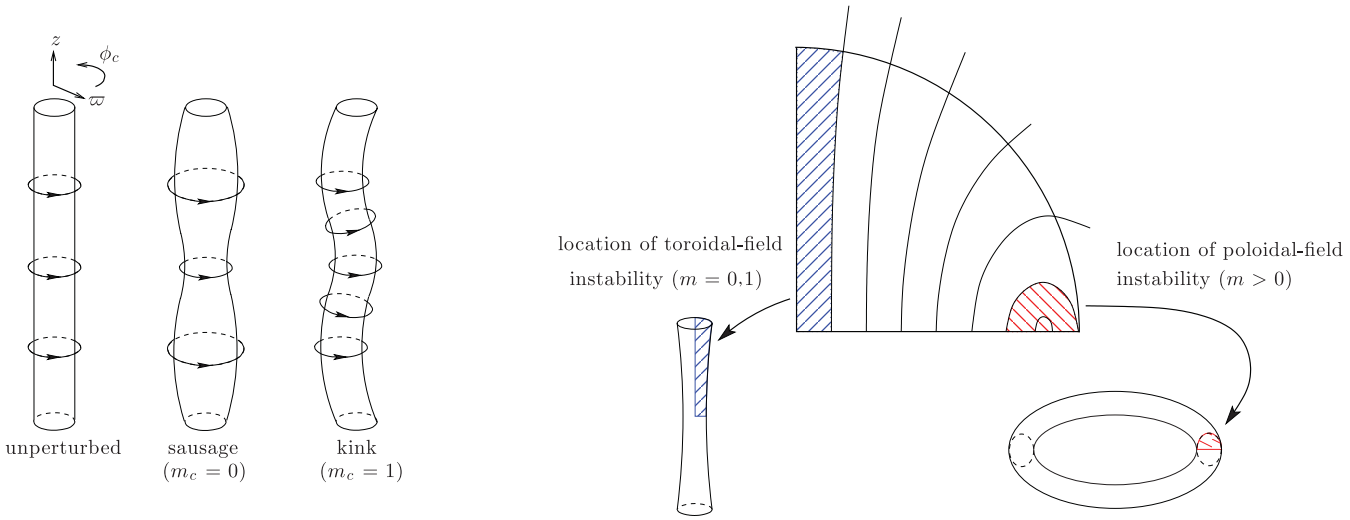

Figure 5. Left: instabilities of a cylindrical plasma column, with field lines in the ϕ_c-direction labelled with arrows. The two main instabilities, in the absence of gravity, are the sausage/varicose mode (with *cylindrical* azimuthal index $m_c = 0$) and the kink mode ($m_c = 1$). Right: the corresponding potentially unstable regions of a mixed-field star – the cylindrical region around the pole, where the toroidal component vanishes, and the torus around the neutral line, where the poloidal component vanishes. The potentially unstable values of m, now accounting for gravity and working in the spherical polar coordinates of the star, are shown.

taken for an Alfvén wave to cross the relevant part of the system. As a diagnostic, we define the following quantity as an order of magnitude estimate for this time:

$$\tau_{\rm A} \equiv \frac{R_*}{\bar{c}_{\rm A}} = R_* \sqrt{\frac{4\pi\bar{\rho}}{\bar{B}^2}}, \tag{25}$$

where $c_{\rm A}$ is the Alfvén speed and overbars denote volume-averaged quantities. To ensure we compare configurations of the same physical field strength, we redimensionalize to typical neutron star parameters (a mass of $1.4\,{\rm M}_\odot$ and a radius $R_* = 10\,{\rm km}$) and take a field strength of $\bar{B} = 3 \times 10^{16}\,{\rm G}$ as our canonical value. The corresponding (dimensionless) Alfvén time-scale $\hat{\tau}_{\rm A} \approx 40$. This strong magnetic field and correspondingly short dynamical time-scale allows for faster numerical evolutions, but we have confirmed our results also hold at lower field strengths. In addition, we have checked that the growth rate of any unstable mode converges with numerical grid resolution, and scales approximately linearly with the magnetic field strength.

Note that confirming the stability of a magnetic field is far more difficult than showing it is unstable: for the latter, one need only find a particular mode with exponential growth in time, whilst for the former, one must establish that *every* potential perturbation results only in innocuous oscillations about the equilibrium and not unstable growth. Within the limitations of our numerics, we are able to test the stability of equilibria against non-axisymmetric initial perturbations with $\mathcal{P}^+$ or $\mathcal{P}^-$ symmetry, up to $m = 6$. Since this test easily shows up instabilities of purely poloidal and purely toroidal fields (Lander & Jones 2011a,b), we may have some confidence that a mixed poloidal–toroidal field showing no such instability is 'stable'. More accurately, it will not be susceptible to the fastest growing class of instabilities and is likely to be dynamically stable; we cannot establish its stability on secular time-scales.

4 STABILITY ANALYSIS OF MIXED-FIELD STARS

4.1 Type 1 (twisted-torus) equilibria

We now begin our analysis of the magnetic stability of barotropic stars containing both poloidal and toroidal field components, using the various background models discussed in Section 2. In particular, we are testing for the possible presence of any instabilities known from the purely poloidal and purely toroidal field cases. In this subsection we test the stability of twisted-torus equilibria (type 1), as constructed in Section 2.1. These equilibria are poloidal-dominated, with a toroidal component only occupying the small volume within the closed-field line region.

In Fig. 6 we compare the stability of a type 1a mixed field with that of a poloidal field. It would be reasonable to expect the addition of a toroidal component to remove, or at least reduce, the instability of the poloidal field (Wright 1973); despite this, our results show *no such* stabilization. On the left-hand side we plot the evolution of perturbed magnetic energy for $\mathcal{P}^+$ (polar) and $\mathcal{P}^-$ (axial) perturbations, on a poloidal-field background. As expected from Section 3.3, the $\mathcal{P}^+$ class evolve stably, whilst the $\mathcal{P}^-$ class suffer an instability that appears at $\hat{t} \approx 30{-}50$; cf. our Alfvén time-scale estimate of $\hat{\tau}_{\rm A} \approx 40$ for this field strength ($\bar{B} = 3 \times 10^{16}\,{\rm G}$).

The right-hand plot shows the corresponding evolutions for a mixed-field star with $\mathcal{E}_{\rm tor}/\mathcal{E}_{\rm mag} = 3\,$per cent, relatively high for a type 1 equilibrium. As for the poloidal field, after one Alfvén time-scale the perturbed magnetic energy grows exponentially; furthermore, since the mixed field breaks the equatorial symmetry of the perturbations (see Section 3.3), even $\mathcal{P}^+$ initial data result in an excitation of unstable modes. The growth rate of the $m = 2$ instability is not reduced by the addition of a toroidal component, nor are the $m = 4$ or 6 instabilities (omitted in Fig. 6 to avoid cluttering it). The $m = 1$ instability, in fact, grows *faster* for a mixed field than for a purely poloidal one. Finally, although we have only plotted

Downloaded from http://mnras.oxfordjournals.org/ at University of Southampton on January 5, 2017

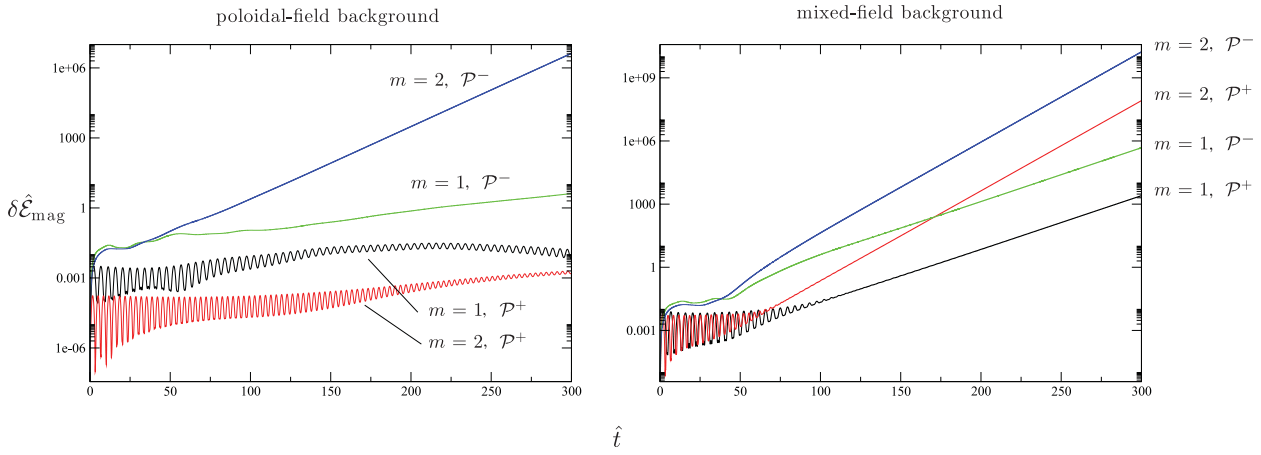

Figure 6. The instability of type 1 (twisted-torus) equilibria; results are shown for type 1a, but the corresponding plots for types 1b and 1c are very similar. Plotting the evolution of the perturbed magnetic energy, we compare the behaviour of $m = 1$ and 2 initial perturbations (with $\mathcal{P}^+$ and $\mathcal{P}^-$ symmetry) in a star with a purely poloidal field (left) and in one where a toroidal component has been added (right). In both cases, unstable growth is seen after approximately one Alfvén time-scale ($\hat{t} \approx 40$ in these dimensionless variables). For the mixed-field star, $\mathcal{E}_{\rm tor}/\mathcal{E}_{\rm mag} = 3$ per cent; this is a high percentage for this class of equilibrium, but nonetheless does not produce any stabilization. For a mixed field, magnetic perturbations across the equator have no definite equatorial symmetry; in a sense, the mixed field allows for 'mixing' of the two $\mathcal{P}$ classes. For this reason, although $\mathcal{P}^+$ initial data start by evolving stably, as for a poloidal-field background, at later times energy is transferred to the unstable class of perturbations.

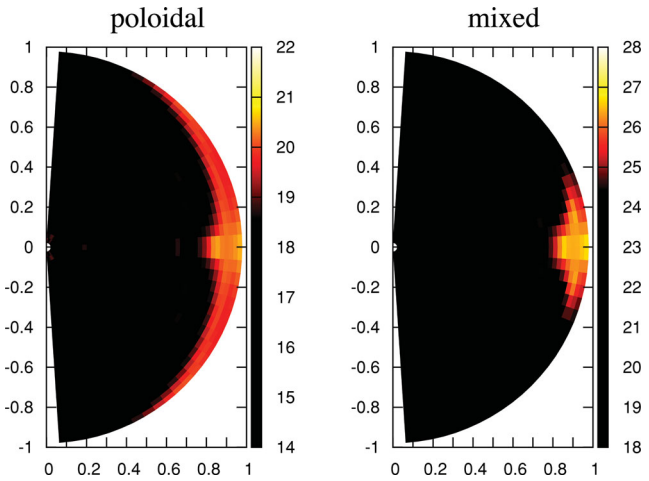

Figure 7. The magnitude of the perturbed magnetic field $|\delta \boldsymbol{B}|$, in logarithmic scale, at late times in the evolution of two stars. The left-hand plot is for $\mathcal{P}^-$ perturbations on a poloidal-field background, whilst the right-hand plot shows perturbations of a mixed field (for which there is no equatorial symmetry); $m = 2$ for both cases. The poloidal-field instability – manifested as exponential growth around the neutral line – is seen to operate in the mixed-field star too. The corresponding plot for $m = 1$ shows similar growth around the neutral line too, with no evidence for additional instabilities originating from the toroidal component of the mixed field.

results for type 1a equilibria, type 1b and type 1c mixed fields are similarly unstable.

Two additional tests help us to confirm that the instability from Fig. 6 is due to the poloidal component. First, we look at its location within the star. In Fig. 7 we plot the magnitude of the perturbed field $|\delta \boldsymbol{B}|$, in the case of a poloidal field and a type 1 mixed configuration. The plots are in logarithmic scale and show the late stages of the evolution, where the unstable mode is completely dominant. For both field configurations shown, there is clear exponential growth around the neutral line – slightly more localized for the mixed field. Although we only show results for $m = 2$, the unstable growth occurs in the same location for $m = 1$, with no indication in this latter case of additional growth due to the potentially unstable toroidal component.

The poloidal-field instability discussed in Section 3.3 should manifest itself as θ-direction motion localized in the closed-field line region. Having confirmed that our instability appears in the expected location, our final test is to study the fluid motion in this region. In Fig. 8 we take a point in the closed-field line region and plot the local ratios of v_θ to v_r and v_θ to v_ϕ over time. The behaviour is consistent with our expectations: after the onset of instability, the θ-direction motion is always more than two orders of magnitude greater than that in either of the other directions.

4.2 Type 2 (confined-field) equilibria

Next we turn to a stability analysis for a star with a confined magnetic field, as described in Section 2.2. This model does not have a twisted-torus structure and is not poloidal-dominated; 65 per cent of its magnetic energy comes from the toroidal component. These differences allow us to explore whether the twisted-torus structure or dominant poloidal field is responsible for the instability of type 1 equilibria.

On the left-hand side of Fig. 9 we plot the evolution of perturbed magnetic energy for $m = 1, 2, 4$ and 6 azimuthal indices. Although the $m = 2, 4$ and 6 instabilities still appear to exist for this magnetic field, their growth rates are greatly reduced in comparison with the type 1 equilibria results. In addition, the onset time for the instabilities is rather longer: about five times that for type 1. One similarity between the type 1 and type 2 results is that the $m = 1$ instability seems to grow more quickly for a mixed field than a purely poloidal one.

Since the type 2 equilibrium is toroidal-dominated, we wish to see which field component is responsible for its instability. Accordingly, on the right-hand side of Fig. 9 we plot $|\delta \boldsymbol{B}|$ throughout the star for an $m = 1$ evolution. We see the fastest unstable growth occurring near the polar surface, indicating that the toroidal component is now unstable (see Section 3.3). There is also substantial growth away from the pole, however, and $m > 1$ perturbations are seen

Downloaded from http://mnras.oxfordjournals.org/ at University of Southampton on January 5, 2017

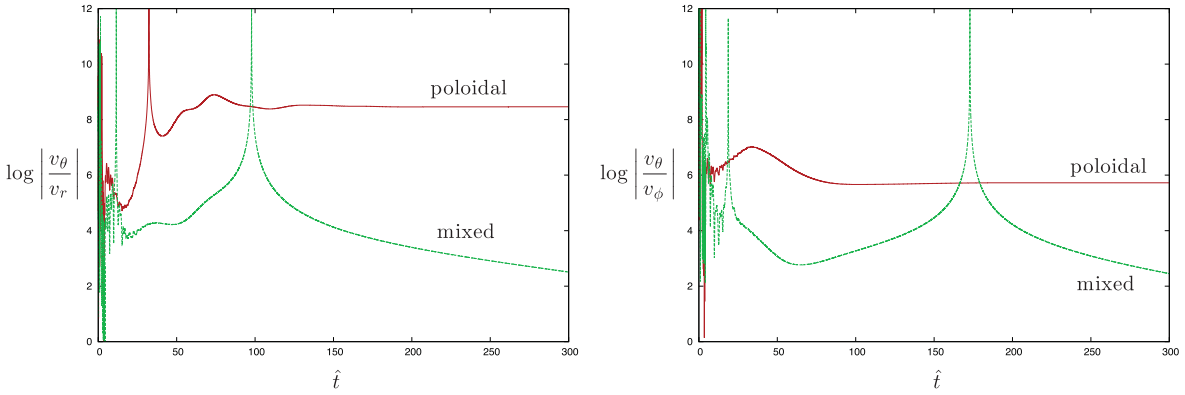

Figure 8. Confirmation that the instability of poloidal and type 1 mixed-field equilibria involves predominantly θ-direction motion. We compare the magnitude of v_θ with that of the other fluid velocity components, for a point in the closed-field line region. The r and ϕ components of the velocity are more significant in the mixed-field configuration than for a purely poloidal-field background, but are still two orders of magnitude weaker than the θ-component.

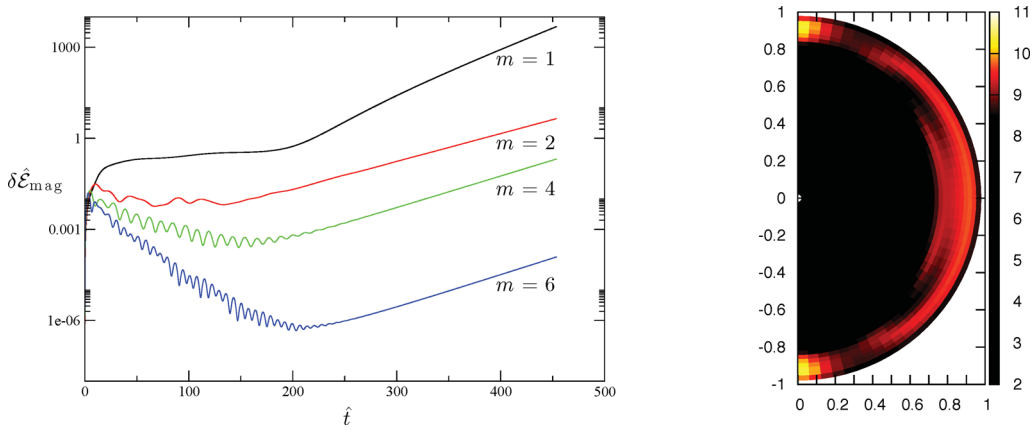

Figure 9. Left: the instability of a confined-field (type 2) equilibrium, seen from the exponential growth of the perturbed magnetic energy in time. The background stellar model is very different from type 1: it is toroidal-dominated ($\mathcal{E}_{\rm tor}/\mathcal{E}_{\rm mag} = 65$ per cent) and does not have a twisted-torus geometry. Although the field strength is the same as before ($\bar{B} = 3 \times 10^{16}$ G), no instabilities manifest themselves until $\hat{t} \approx 200$ – five times our estimated Alfvén time-scale. Right: the unstable growth in $|\delta \boldsymbol{B}|$ is fastest around the pole, suggesting that the toroidal component is the main origin of the instability for type 2 equilibria.

to be unstable too; both of these results indicate that the poloidal component also plays a role in the instability of this field type.

4.3 Type 3 (surface-current) equilibria

In this subsection we test the stability of type 3 equilibria, our final class of mixed-field configurations, where we have an exterior poloidal field but nonetheless a strong toroidal component. This is achieved by allowing for a step in the toroidal component at the surface and requires a corresponding surface current. Recall, however, that we are not able to study the surface dynamics of the perturbed magnetic field directly, since we evolve the flux variable $\beta = \rho_0 \delta \boldsymbol{B}$.

We consider two examples of surface-current equilibria, type 3a and type 3b, as described in Section 2.3. Both have substantial toroidal components, with comparable energy to the poloidal component: for type 3a $\mathcal{E}_{\rm tor}/\mathcal{E}_{\rm mag} = 50$ per cent, and for type 3b $\mathcal{E}_{\rm tor}/\mathcal{E}_{\rm mag} = 30$ per cent. In each case, the value was the upper limit on the percentage of toroidal field possible with our chosen functional forms. From Fig. 10 we see some degree of stabilization in these equilibria, compared with those of type 1. In the evolution for type 3b, the $m = 6$ instability appears to have been removed and the $m = 4$ instability considerably reduced. However, the $m = 1$ and 2 instabilities remain.

Type 3a is the closest to a stable barotropic equilibrium we have found, with no evidence for the existence of $m = 2$, 4 or 6 instabilities. Despite this, we still see exponential growth for $m = 1$ – which is enough to render this magnetic field unstable. Given the stabilization of other modes, one might question whether the $m = 1$ growth is numerical rather than physical in origin. We have checked this, as for all other unstable configurations, by convergence-testing the instability growth rate. Furthermore, the unstable growth was localized around the neutral line, closely resembling the plots in Fig. 7. This suggests an instability of physical origin, related to the poloidal component of the magnetic field, even though the toroidal component contributes 50 per cent of the magnetic energy.

4.4 Rotation

We conclude our stability analysis by looking at the effect of rotation. Rotation may act to reduce magnetic instabilities, though there is some uncertainty in the literature about how effective the stabilization will be. Part of the problem is that there are no conclusive analytic results for the rotating case, due to the increased complexity of the stability conditions (Frieman & Rotenberg 1960;

Downloaded from http://mnras.oxfordjournals.org/ at University of Southampton on January 5, 2017

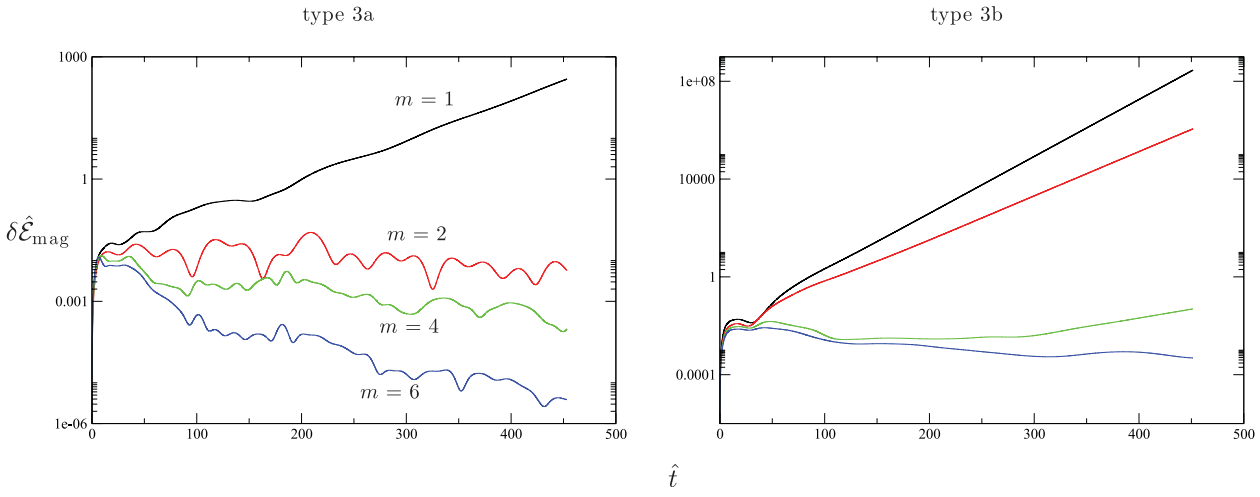

Figure 10. Behaviour of $m = 1, 2, 4$ and 6 perturbations on background equilibria with surface currents and fairly high percentages of toroidal-field energy (50 per cent for type 3a, 30 per cent for type 3b). We see that higher m modes are stabilized, but the $m = 1$ poloidal-field instability is not removed even in the case of 50 per cent toroidal energy.

Lynden-Bell & Ostriker 1967; Glampedakis & Andersson 2007) with respect to the static case (Bernstein et al. 1958).

Although no definitive analytic results exist for the stability of rotating magnetized stars, the work of Pitts & Tayler (1985) provides some suggestions, based on approximate treatments of some model problems. They predict that rapid rotation may remove magnetic instabilities already present in the non-rotating star, but that a new instability will be introduced, albeit one with a lower growth rate. From numerical studies, there seems to be agreement that rotation can reduce toroidal-field instabilities (Braithwaite 2006; Kitchatinov & Rüdiger 2008; Kiuchi, Yoshida & Shibata 2011; Lander & Jones 2011a), though it cannot necessarily provide complete stabilization. For poloidal fields, Geppert & Rheinhardt (2006) and Lander & Jones (2011b) find that rotation has some stabilizing effect, whilst Braithwaite (2007) does not. With somewhat tentative expectations, we now turn to our results for a rotating star with a mixed poloidal–toroidal field. We focus on $m = 2$ perturbations on a type 1a mixed-field background in this subsection, but the results are representative of other field types and perturbations we have tested.

To study the effect of rotation on magnetic instabilities, we monitor the evolution of the perturbed magnetic energy once again. We quantify the (exponential) instability growth rate using the parameter

$$\zeta \equiv \frac{1}{\Delta t}\Delta\left[\ln\left(\frac{\delta\mathcal{E}_{\rm mag}}{\mathcal{E}_{\rm mag\,0}}\right)\right]. \tag{26}$$

From the left-hand plot of Fig. 11 we find that rotation certainly decreases the growth rate of the perturbations, although some degree of unstable growth is present in all results. Our code suffers some numerical instabilities for very rapidly rotating stars, so the highest rotation rate we include here is 57 per cent of the Keplerian value.

The work of Pitts & Tayler (1985) suggests that a non-rotating star's magnetic instabilities should be suppressed when the rotational angular velocity exceeds the corresponding Alfvén velocity $\Omega_{\rm A} \approx 2\pi/\tau_{\rm A}$. Using our previous estimate for $\tau_{\rm A}$ (25), we expect this suppression to occur at $\hat{\Omega} \approx 0.11$ for $\bar{B} = 2.25 \times 10^{16}$ G and at $\hat{\Omega} \approx 0.14$ for $\bar{B} = 3 \times 10^{16}$ G. As the original instability is removed, however, Pitts & Tayler (1985) predict a new instability will be induced whose growth rate may be slower but still significant.

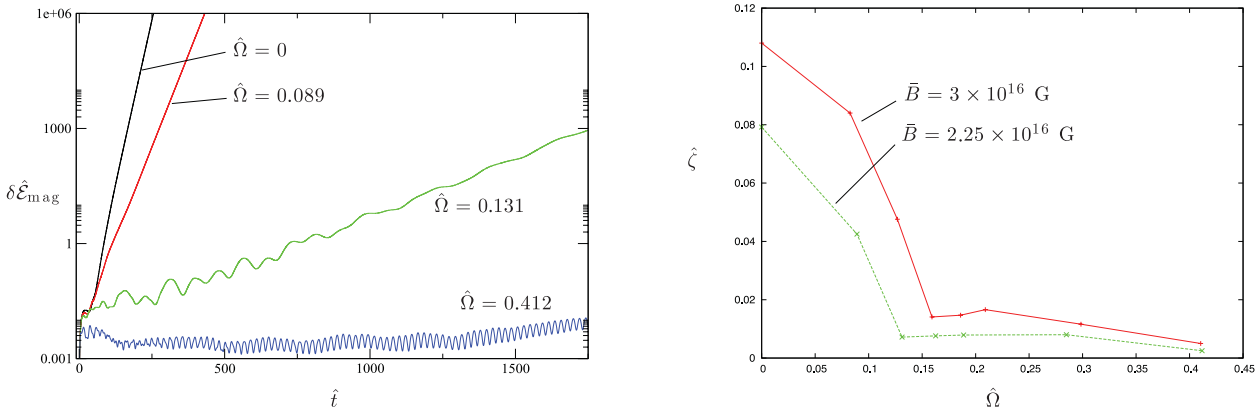

Figure 11. Left: the evolution of the perturbed magnetic energy in a rotating mixed-field star, for different dimensionless rotation rates. Rotation is seen to reduce, but not remove, the instability. Note that the Keplerian frequency in these units $\hat{\Omega}_{\rm K} \approx 0.72$. Numerical instability prevents us from studying more rapidly rotating stellar models than $\hat{\Omega} = 0.412$, around 57 per cent of the Keplerian value. Right: instability growth rate ζ as a function of rotation rate, for two field strengths. The instability present for $\Omega = 0$ seems to be reduced by rotation, but at around $\hat{\Omega} = 0.15$ the lines plateau, suggesting the appearance of a second instability.

Downloaded from http://mnras.oxfordjournals.org/ at University of Southampton on January 5, 2017

With these results in mind, we now turn to the right-hand plot of Fig. 11. Here we quantify the effect of rotation, plotting the rate of exponential growth of the magnetic energy as a function of rotation rate. We consider stars with $\bar{B} = 2.25$ and 3×10^{16} G (a ratio of 3:4) to investigate the scaling of instability growth rate with field strength. At zero rotation rate the more highly magnetized star has a growth rate 4/3 that of the other, confirming the linear dependence we expect in this case. Adding rotation causes an initial decrease in growth rate which is roughly linear in Ω, up to some threshold value: $\hat{\Omega} \approx 0.13$ for the weaker magnetic field, $\hat{\Omega} \approx 0.16$ for the stronger field. These values agree rather well with the estimates of the previous paragraph. Beyond the threshold rotation rate for each star, the unstable growth rate seems to reach a plateau value of $\sim$10 per cent that of the non-rotating case. We believe this corresponds to the new magneto-inertial instability predicted to occur for sufficiently rapid rotation.

5 DISCUSSION: POSSIBLE STABLE EQUILIBRIA

The aim of this paper has been to construct as wide a range of mixed poloidal–toroidal magnetic fields as possible in barotropic stars, and then to test their stability. We have found that *all* of these equilibria are unstable: poloidal-dominated twisted-torus models (like those of Tomimura & Eriguchi 2005, Lander & Jones 2009 and Ciolfi et al. 2009), toroidal-dominated fields confined within the star (Haskell et al. 2008; Duez & Mathis 2010) and equilibria with surface currents (Colaiuda et al. 2008). For equilibria where $\mathcal{E}_{\rm tor}/\mathcal{E}_{\rm mag} \leq 50$ per cent, the instability's origin appeared to be the poloidal component; for the confined-field model we tested, with $\mathcal{E}_{\rm tor}/\mathcal{E}_{\rm mag} = 65$ per cent, we found evidence of a toroidal-field instability, but some indications of instability in the poloidal component too. This seems to leave little scope for configurations where all magnetic instabilities are suppressed. On the other hand, we have observational evidence for long-lived stellar magnetic fields, so stable magnetic equilibria clearly exist. Here we discuss possible mechanisms to suppress the instabilities we have found.

Rotation: highly magnetized stars (like many Ap/Bp stars, magnetic white dwarfs and magnetars) often rotate relatively slowly. In some, however, the kinetic rotational energy greatly exceeds the magnetic energy and one might expect suppression of magnetic instabilities. We find, however, that when rotation seems rapid enough to suppress the original magnetic instability (of a non-rotating star), a new instability appears to be introduced. This new magneto-inertial instability has a growth rate of $\sim$10 per cent the non-rotating value – still very short on stellar time-scales.

Non-axisymmetry: our code uses a decomposition of the perturbation equations in the azimuthal angle, which relies on having an axisymmetric background star. It is possible that a non-axisymmetric magnetic field will not suffer from the same instabilities we have found. Indeed, the non-linear evolutions of Lasky et al. (2011) and Ciolfi et al. (2011) seem to show unstable initial fields developing non-axisymmetric structure. At the end of these reported simulations, however, the field remains highly dynamic in the closed-field line region, so it is probably too early to regard the results as stable equilibria. It would be very interesting to see whether these fields settle down over longer evolution times.

Stratification: perhaps the easiest way to explain our results is to say that they are irrelevant for real stars, where the equation of state is not barotropic but instead stratified. Indeed, the only numerical evolutions which seem to produce stable magnetic equilibria use a stratified stellar model, where the stratification is due to temperature/entropy gradients (Braithwaite & Nordlund 2006; Braithwaite 2009). Whether these equilibria are, in fact, stable is not completely settled: Bonanno & Urpin (2011) discuss a generic magnetic instability whose lengthscale can be very short, and hence may not show up in numerical simulations (for which the grid is necessarily relatively coarse).

In any case, results for entropy-based stratification may not be applicable to neutron stars, where the stratification comes from composition gradients. Recently, some first attempts have been made to model such equilibria (Mastrano et al. 2011; Glampedakis, Andersson & Lander 2012; Lander, Andersson & Glampedakis 2012), but these are qualitatively similar to barotropic results and their stability is unknown. Note that there is no guarantee that *radial* stratification will suppress the instabilities we find, which mainly involve θ-direction motion (although it does appear to in Braithwaite & Nordlund 2006 and related papers).

Elastic crust: in the case of neutron stars, the outermost layer of the star (around a kilometre in thickness) consists of an elastic crust. This crust *does* have the potential to suppress unstable motion of the kind studied in this paper, up to some critical field strength roughly corresponding to when the magnetic energy exceeds the crustal elastic energy. The precise value depends on the poorly known yield strain of the crust, but is estimated at around 10^{14} G (Thompson & Duncan 1993). Above this field strength, a magnetic instability can cause the crust to crack, which is a plausible scenario for the triggering of magnetar bursts (Thompson & Duncan 1995). For white dwarfs and Ap/Bp stars, there is no analogous outer region to hold an unstable field in place.

Superconductivity: relatively little is known about the equilibria and stability of magnetic fields in superconducting stars. The magnetic force takes a very different form from the normal Lorentz force, however, so it is not unreasonable to expect significant differences in the magnetic field configurations too (Mendell 1998; Glampedakis, Andersson & Samuelsson 2011). Neutron stars quickly become cool enough to contain superconducting regions (Page et al. 2011; Shternin et al. 2011), so this aspect of their physics may help stabilize (or destabilize!) their magnetic fields.

6 SUMMARY

We construct a wide range of barotropic stellar equilibria, with mixed poloidal–toroidal magnetic fields. These include poloidal-dominated and toroidal-dominated configurations, as well as those where both components have comparable energies. Every field configuration is found to suffer instabilities whose origin appears to be one of the two field components. Starting with a poloidal-dominated field, increasing the strength of the toroidal component suppresses unstable poloidal-component modes of higher azimuthal number, but the $m = 1$ instability is difficult to remove. For a sufficiently strong toroidal component, the origin of the $m = 1$ instability appears to change from the poloidal to the toroidal component. Rotation reduces the instability growth rate, but seems to introduce a new instability of slightly weaker growth rate (around 10 per cent of the non-rotating value).

Although this paper does not *prove* the non-existence of stable fields in barotropic stars, it suggests that any such fields form – at best – a very restricted set (which we have been unable to obtain). By contrast, many classes of stars are observed to have long-lived magnetic fields, so we expect that stable magnetic equilibria do exist. Our results indicate that barotropic models may, therefore, be of limited astrophysical relevance. For main-sequence stellar models, the addition of entropy-gradient stratification seems to allow for

Downloaded from http://mnras.oxfordjournals.org/ at University of Southampton on January 5, 2017

stable equilibria, and the same may then be true for white dwarfs. For the modelling of neutron star fields, we believe that it is now particularly important to account for additional physics beyond the barotropic fluid model, including the effect of a crust, composition gradients and superconductivity.

ACKNOWLEDGMENTS

We thank Kostas Glampedakis for useful discussions during this project and Bryn Haskell, Paul Lasky and Burkhard Zink for clarifying aspects of their work. We are also grateful to the referee for helpful criticism. SKL is supported by the German Science Foundation (DFG) via SFB/TR7 and DIJ by STFC via grant number ST/H002359/1. We acknowledge additional support from CompStar, an ESF research networking programme.

REFERENCES

Bernstein I. B., Frieman E. A., Kruskal M. D., Kulsrud R. M., 1958, Proc. R. Soc. London A, 244, 17
Bonanno A., Urpin V., 2011, Phys. Rev. E, 84, 056310
Bonazzola S., Gourgoulhon E., 1996, A&A, 312, 675
Braithwaite J., 2006, A&A, 453, 687
Braithwaite J., 2007, A&A, 469, 275
Braithwaite J., 2009, MNRAS, 397, 763
Braithwaite J., Nordlund Å., 2006, A&A, 450, 1077
Chandrasekhar S., Fermi E., 1953, ApJ, 118, 116
Ciolfi R., Ferrari V., Gualtieri L., Pons J. A., 2009, MNRAS, 397, 913
Ciolfi R., Ferrari V., Gualtieri L., 2010, MNRAS, 406, 2540
Ciolfi R., Lander S. K., Manca G. M., Rezzolla L., 2011, ApJ, 736, L6
Colaiuda A., Ferrari V., Gualtieri L., Pons J. A., 2008, MNRAS, 385, 2080
Dedner A., Kemm F., Kröner D., Munz C.-D., Schnitzer T., Wesenberg M., 2002, J. Comput. Phys., 175, 645
Donati J.-F., Landstreet J. D., 2009, ARA&A, 47, 333
Duez V., Mathis S., 2010, A&A, 517, A58
Frieman E., Rotenberg M., 1960, Rev. Modern Phys., 32, 898
Geppert U., Rheinhardt M., 2006, A&A, 456, 639
Glampedakis K., Andersson N., 2007, MNRAS, 377, 630
Glampedakis K., Andersson N., Samuelsson L., 2011, MNRAS, 410, 805
Glampedakis K., Andersson N., Lander S. K., 2012, MNRAS, 420, 1263
Grad H., Rubin H., 1958, in Proc. 2nd United Nations Int. Conf. on Peaceful Uses of Atomic Energy, Vol. 31. United Nations, Geneva, p. 190
Harding A. K., Lai D., 2006, Rep. Progress Phys., 69, 2631
Haskell B., Samuelsson L., Glampedakis K., Andersson N., 2008, MNRAS, 385, 531
Ioka K., 2001, MNRAS, 327, 639
Kitchatinov L. L., Rüdiger G., 2008, A&A, 478, 1
Kiuchi K., Yoshida S., Shibata M., 2011, A&A, 532, A30
Lander S. K., Jones D. I., 2009, MNRAS, 395, 2162
Lander S. K., Jones D. I., 2011a, MNRAS, 412, 1394
Lander S. K., Jones D. I., 2011b, MNRAS, 412, 1730
Lander S. K., Jones D. I., Passamonti A., 2010, MNRAS, 405, 318
Lander S. K., Andersson N., Glampedakis K., 2012, MNRAS, 419, 732
Lasky P. D., Zink B., Kokkotas K. D., Glampedakis K., 2011, ApJ, 735, L20
Lynden Bell D., Ostriker J. P., 1967, MNRAS, 136, 293
Lyutikov M., 2010, MNRAS, 402, 345
Markey P., Tayler R. J., 1969, MNRAS, 145, 217
Markey P., Tayler R. J., 1973, MNRAS, 163, 77
Mastrano A., Melatos A., Reisenegger A., Akgün T., 2011, MNRAS, 417, 2288
Mendell G., 1998, MNRAS, 296, 903
Mestel L., 1956, MNRAS, 116, 324
Mestel L., 1999, Stellar Magnetism. Clarendon Press, Oxford
Page D., Prakash M., Lattimer J. M., Steiner A. W., 2011, Phys. Rev. Lett., 106, 081101
Pitts E., Tayler R. J., 1985, MNRAS, 216, 139
Reisenegger A., 2009, A&A, 499, 557
Reisenegger A., Goldreich P., 1992, ApJ, 395, 240
Shafranov V. D., 1958, Soviet J. Exp. Theor. Phys, 6, 545
Shternin P. S., Yakovlev D. G., Heinke C. O., Ho W. C. G., Patnaude D. J., 2011, MNRAS, 412, L108
Tayler R. J., 1973, MNRAS, 161, 365
Tayler R. J., 1980, MNRAS, 191, 151
Thompson C., Duncan R. C., 1993, ApJ, 408, 194
Thompson C., Duncan R. C., 1995, MNRAS, 275, 255
Tomimura Y., Eriguchi Y., 2005, MNRAS, 359, 1117
Wickramasinghe D. T., Ferrario L., 2000, PASP, 112, 873
Wright G. A. E., 1973, MNRAS, 162, 339

This paper has been typeset from a TEX/LATEX file prepared by the author.

Downloaded from http://mnras.oxfordjournals.org/ at University of Southampton on January 5, 2017